Structural diversity in layered hybrid perovskites, A2PbBr4 or AA'PbBr4, templated by small disc-shaped amines

Journal:	*Inorganic Chemistry*
Manuscript ID	ic-2020-01807g.R1
Manuscript Type:	Article
Date Submitted by the Author:	20-Jul-2020
Complete List of Authors:	Guo, Yuan-Yuan; University of Saint Andrews, Chemistry Yang, Linjie; University of Saint Andrews, Chemistry Biberger, Simon; University of Bayreuth, Physics McNulty, Jason; University of Saint Andrews, Chemistry Li, Teng; University of Saint Andrews, Chemistry Schoetz, Konstantin; University of Bayreuth, Physics Panzer, Fabian; Universitat Bayreuth, Soft Matter Optoelectronics Lightfoot, Philip; University of Saint Andrews, Chemistry

Structural diversity in layered hybrid perovskites, A_2PbBr_4 or $AA'PbBr_4$, templated by small disc-shaped amines

Yuan-Yuan Guo,[†] Lin-Jie Yang,[†] Simon Biberger,[§] Jason A. McNulty,[†] Teng Li,[†] Konstantin Schötz,[§] Fabian Panzer,[§] and Philip Lightfoot*[,†]

[†]School of Chemistry and EaStChem, University of St Andrews, St Andrews, KY16 9ST, United Kingdom

[§]Soft Matter Optoelectronics, Department of Physics, University of Bayreuth, 95440 Bayreuth, Germany

*e-mail: pl@st-andrews.ac.uk

Abstract

We present three new hybrid layered lead(II) bromide perovskites of generic composition A_2PbBr_4 or $AA'PbBr_4$, which exhibit three distinct structure types. $[TzH]_2PbBr_4$, ($[TzH^+]$ = 1,2,4-triazolium), adopts a (001)-oriented layer structure, $[AaH]_2PbBr_4$, ($[AaH^+]$ = acetamidinium), adopts a (110)-oriented type, whereas $[ImH][TzH]PbBr_4$, ($[ImH^+]$ = imidazolium), adopts a rare (110)-oriented structure with enhanced corrugation (*i.e.* '3 × 3' type). The crystal structures of each are discussed in terms of the differing nature of the templating molecular species. Photoluminescent spectra for each are reported and the behaviours discussed in relation to the different structure of each composition.

Introduction

The promising photophysical properties and enormous chemical and structural diversity shown by lead(Ⅱ) halide perovskites (LHPs) has led to a considerable amount of exploratory synthetic work in this field.[1,2] Amongst these, lower dimensional layered perovskites can be imagined as structural derivatives of the ABX_3 composition aristotype cubic perovskite structure, formed by slicing along specific crystallographic directions, and inserting additional moieties between these layers. Thus, the (001)-oriented perovskites can be regarded as derived from 'slicing' along the (001) planes of the parent perovskite structure as shown in Figure 1a, resulting in '*trans*' ligands of the octahedral framework being terminal. The (001)-oriented layered perovskites are evidently particularly tolerant not only to inorganic but also organic *inter*-layer

components, producing a great diversity of compositional and structural variants. A related series of layered structure types, the (110)-oriented layered perovskites, can be regarded as derived from the parent ABX_3 perovskite by slicing along (110) planes, resulting in '*cis*' ligands of the octahedral framework being terminal. Depending on the degree of 'corrugation' which occurs within the layers, these structures can be described as 2 × 2, 3 × 3 *etc*., as shown in Figure 1b.[3]

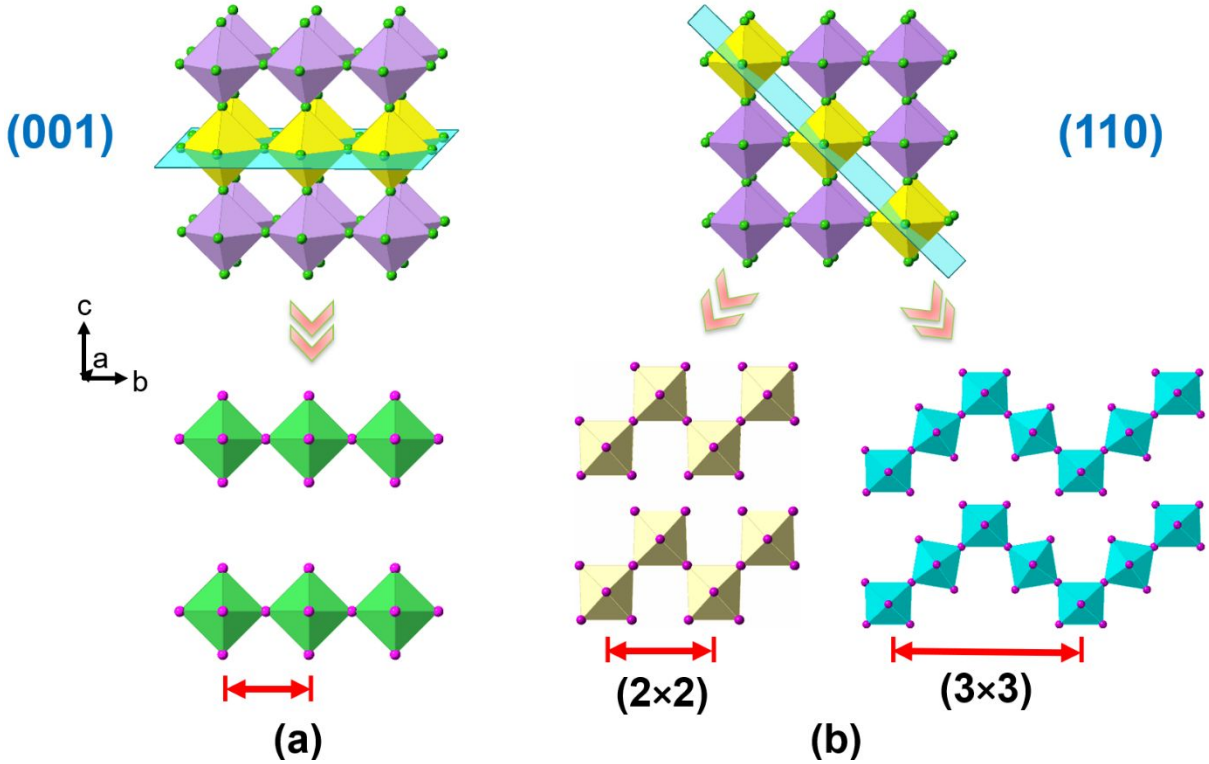

Figure 1. Schematic dimensional reduction of parent cubic perovskite to (a) (001)-oriented and (b) (110)-oriented layered perovskites.

A further degree of variability, common to each of these generic families, is that it is feasible to incorporate either one or two distinct cations in the *inter*-layer region, leading to generic compositions ABX_4 or $AA'BX_4$ (in the case of a single octahedral layer). Manipulations at the A and A′ sites can obviously lead to consequent modifications to the arrangement of the perovskite-like layers themselves, thus helping to tailor the resultant physical properties. In the case of the (001)-oriented layers and in the field of purely inorganic perovskites, the two generic families are the well-known Dion-Jacobson (DJ)[4] and Ruddlesden-Popper (RP)[5] series, having stoichiometries ABX_4 and $AA'BX_4$, respectively for examples with single octahedral layers. The corresponding inorganic-only (110)-oriented phases are much less common.[6] Indeed, the same can be said of the corresponding LHPs, where there are now countless examples of the (001)-type,[2] but still only a handful of the various (110)-types.[2,7–9] In the case

of LHPs, the ABX_4 variant must contain a single divalent organo-cation, whereas the $AA'BX_4$ analogue will contain two (same or distinct) monovalent organic cations.[7]

In our previous work,[7] we reported two examples of the latter series, *i.e* the 2 × 2 (110)-oriented structure type. We specifically chose two similarly sized, 'disc-shaped' mono-protonated amines, in order to explore structure-directing effects, based on both size and H-bonding preferences, to produce [ImH][GuH]$PbBr_4$ (″IGPbBr_4″) and [TzH][GuH]$PbBr_4$ (″TGPbBr_4″); [ImH^+] = imidazolium, [TzH^+] = 1,2,4-triazolium, [GuH^+] = guanidinium). In the present work, we present another three new $AA'BX_4$ type LHPs: $[TzH]_2PbBr_4$ (″T_2PbBr_4″), $[AaH]_2PbBr_4$ (″A_2PbBr_4″; [AaH^+] = acetamidinium), and [ImH][TzH]$PbBr_4$ (″ITPbBr_4″). Interestingly, they adopt three different structure types, *viz*. (001) for T_2PbBr_4, 2 × 2 (110) for A_2PbBr_4, and 3 × 3 (110) for ITPbBr_4. The crystal structures are discussed in detail in order to inform future considerations of the 'designability' of these various structure types.

Experimental Section

Synthesis

1,2,4-triazole ($C_2H_3N_3$, 99%), acetamidine hydrochloride, ($C_2H_6N_2$·HCl, 97%), imidazole ($C_3H_4N_2$, 99%), lead (II) bromide ($PbBr_2$, ≥98%) and hydrobromic acid (HBr, 48%, w/w aqueous solution), were purchased from Alfa Aesar. Diethyl ether ($(C_2H_5)_2O$, 99.5%) was purchased from Sigma Aldrich. All chemicals were directly used without further purification.

The title compounds, T_2PbBr_4, A_2PbBr_4 and ITPbBr_4 were crystallized by a slow evaporation method.

T_2PbBr_4 ($C_4H_8N_6PbBr_4$), 1,2,4-triazole (276 mg, 4 mmol) and $PbBr_2$ (734 mg, 2 mmol) were dissolved in conc. HBr (3 mL) with moderate heating. By cooling for a few hours, bright yellow, plate-shaped crystals were obtained. These crystals were filtered and washed with diethyl ether (yield 48% based on $PbBr_2$). Elemental analysis: (Anal. Calc. (%) for T_2PbBr_4: C, 7.20; H, 1.21; N, 12.60. Found: C, 7.37; H, 1.15; N, 12.53).

A_2PbBr_4 ($C_4H_{14}N_4PbBr_4$), Acetamidine hydrochloride (1890 mg, 20 mmol) and $PbBr_2$ (734 mg, 2 mmol) were dissolved in conc. HBr (6 mL) with moderate heating. By cooling for a few hours, colorless, plate-shaped crystals were obtained. These crystals were filtered and washed with diethyl ether (yield 41% based on $PbBr_2$). Elemental analysis: (Anal. Calc. (%) for A_2PbBr_4: C, 7.45; H, 2.19; N, 8.69. Found: C, 7.53; H, 2.11; N, 8.73).

$ITPbBr_4$ ($C_5H_9N_5PbBr_4$), imidazole (136 mg, 2 mmol), 1,2,4-triazole (138 mg, 2 mmol) and $PbBr_2$ (734 mg, 2 mmol) were dissolved in conc. HBr (4 mL) with moderate heating. By cooling for a few hours, pale yellow, needle-shaped crystals were obtained. These crystals were filtered and washed with diethyl ether (yield 40% based on $PbBr_2$). Elemental analysis: (Anal. Calc. (%) for $ITPbBr_4$: C, 9.02; H, 1.36; N, 10.52. Found: C, 8.94; H, 1.22; N, 10.54).

Characterization

Single crystal X-ray diffraction data were collected at 173 K and 298 K on a Rigaku SCX Mini diffractometer using Mo-K_α radiation. Data were collected using CrystalClear (Rigaku) software.[10] Structures were solved by direct methods using SHELXT,[11] and full-matrix least-squares refinements on F^2 were carried out using SHELXL-2018/3[11] incorporated in the WinGX program.[12] Absorption corrections were performed empirically from equivalent reflections on the basis of multi-scans by using CrystalClear.[10] Non-H atoms were refined anisotropically and hydrogen atoms were treated as riding atoms. Powder X-ray diffraction data were collected on a PANalytical EMPYREAN diffractometer using Cu $K_{\alpha1}$ (λ = 1.5406 Å) radiation in the range of 3 to 70° to confirm the purity of each sample. Ambient temperature solid UV-Vis absorbance spectra of powder T_2PbBr_4, A_2PbBr_4 and $ITPbBr_4$ were collected on a JASCO-V550 ultraviolet–visible spectrophotometer with the wavelength range at 200 nm to 900 nm. Temperature dependent steady-state PL measurements were carried out on powdered pellet samples of T_2PbBr_4, $ITPbBr_4$ and A_2PbBr_4 using a home-built setup, that is described in more detail elsewhere.[13] In brief, the pellets were placed in a continuous flow cryostat (Oxford Instruments, Optistat CF) connected to a temperature controller (Oxford Instruments ITC503S) and the sample was excited with a pulsed 337 nm nitrogen laser (LTB MNL 100). The PL-signal was detected by a spectrograph (Andor Shamrock SR3030i) coupled to a CCD-camera (Andor iDus420a-OE). For PLQY measurements, we used the method described by de Mello *et al*.[14] The samples were excited using a 375 nm diode laser by PicoQuant and the spectra were recorded with a CCD-camera (Andor DU420A-OE).

Results and Discussion

Crystal Structures

The single crystal X-ray structures suggest no phase transitions in the regime 173 < T < 298 K, so the crystallographic details will be discussed based on the structures at 298 K. Details of the structures at 173 K are provided in ESI. Crystallographic parameters for all three structures at 298 K are given in Table 1.

Table 1. Crystal and Structure Refinement Data at 298 K

	T_2PbBr_4	A_2PbBr_4	$ITPbBr_4$
Formula	$C_4H_8N_6PbBr_4$	$C_4H_{14}N_4PbBr_4$	$C_5H_9N_5PbBr_4$
Formula weight	666.99	645.02	666.00
Colour/Habit	Yellow/Block	Colorless/Block	Colorless/Prism
Crystal size (mm^3)	0.23 × 0.17 × 0.09	0.22 × 0.18 × 0.13	0.21 × 0.12 × 0.11
Crystal system	Monoclinic	Monoclinic	Orthorhombic
Space group	*C*2/*c*	$P2_1/c$	*Pbcm*
***a* (Å)**	11.9243(9)	12.6949(9)	6.0154(5)
***b* (Å)**	11.9327(9)	9.2998(7)	25.873(2)
***c* (Å)**	19.3394(15)	12.2739(7)	18.9242(17
α (°)	90	90	90
β (°)	95.212(6)	90.996(6)	90
γ (°)	90	90	90
***V* ($Å^3$)**	2740.4(4)	1448.84(18)	2945.3(4)
Z	8	4	8
ρ_{calc} (g/cm^3)	3.233	2.957	3.004
μ (mm^{-1})	23.958	22.648	22.289
F(000)	2368	1152	2368
Reflns collected	11310	14371	23202
Independent reflns	2394 [R(int) = 0.0545]	3294 [R(int) = 0.0478]	2664 [R(int) = 0.0834]
Goodness of Fit	0.939	0.939	0.94
Final *R* indices ($I > 2\sigma(I)$)	R_1 = 0.0245 wR_2 = 0.0538	R_1 = 0.0233 wR_2 = 0.0459	R_1 = 0.0259 wR_2 = 0.0537
Largest diff. peak/hole (e $Å^{-3}$)	1.504/-1.513	0.956/-1.224	1.028/-1.656

T_2PbBr_4

T_2PbBr_4 crystallises in a (001)-oriented structure type (Figure 2). Whilst octahedral tilting occurs within each $[PbBr_4]_\infty$ layer, adjacent octahedral layers occur in an almost 'eclipsed' conformation relative to each other, which resembles the DJ rather than the RP family, despite the A_2BX_4 stoichiometry. We note that there is currently controversy regarding the naming of families of layered hybrid perovskites in relation to structural and compositional features[15]

though in terms of describing and comparing structural distortions within the inorganic layers in these materials, such comparisons can be helpful. Although the original naming of the RP and DJ phases referred to compositional differences, $A_2'A_{n-1}B_nO_{3n+1}$ and $A'A_{n-1}B_nO_{3n+1}$, respectively, a more useful distinction in the context of LHPs regards the nature and degree of 'staggering' of adjacent perovskite-like octahedral layers. Here, we choose to describe the present structure as related to the DJ family, despite the compositional resemblance to the RP family, as the octahedral layers are almost eclipsed.

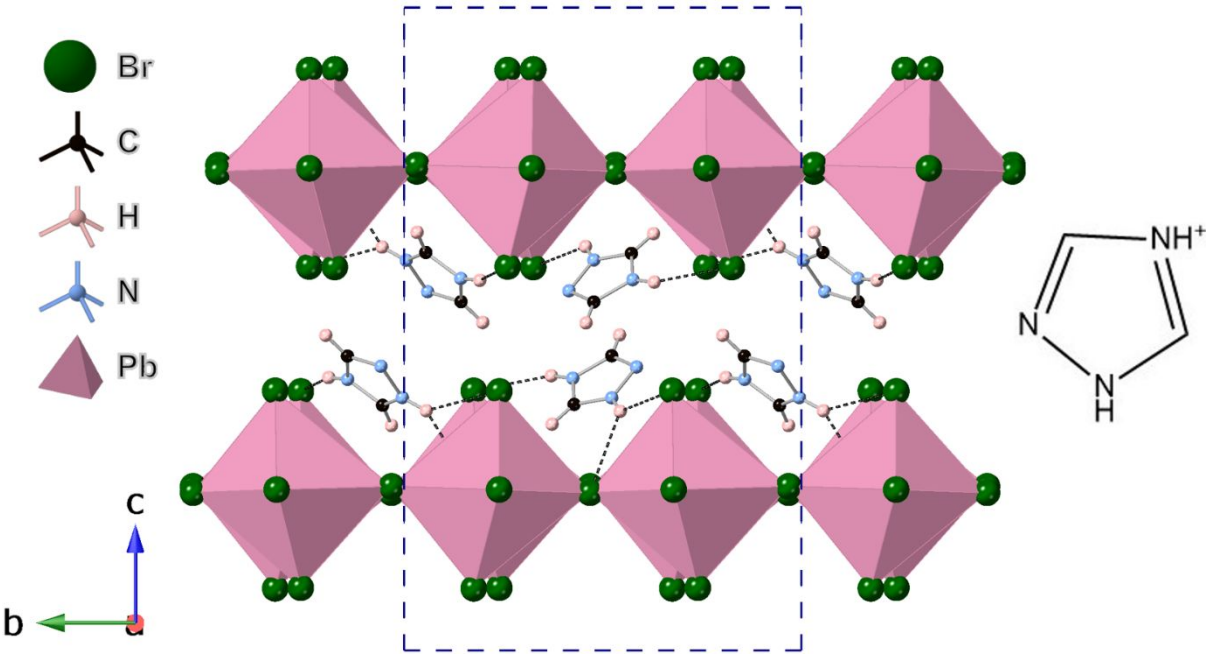

Figure 2. Crystal structure of T_2PbBr_4.

The unit cell of T_2PbBr_4 has a $2a_p \times 2a_p \times 2c_p$ supercell relative to the parent DJ structure ($TlAlF_4$), which is caused by a combination of octahedral tilting/distortion together with ordering of [TzH^+] cations over two distinct sites and the cooperative minor staggering of adjacent octahedral layers. Figure 2 shows the packing arrangement, together with the H-bonding of the [TzH^+] moieties to the inorganic layers. The driving force for this expanded supercell may be broken down into the effects of octahedral tilting together with the effects of the arrangement of the organic species. In the notation used by Li *et al.*[16] the tilt system of T_2PbBr_4 is an unusual one: a^-b^0c, signifying rotation of octahedra around the *c*-axis and out-of-phase tilting of adjacent octahedra along *only one* of the in-plane axes. These tilt modes acting alone would lead to a supercell $2a_p \times 2a_p \times c_p$ in space group *C*2/*m*, with perfectly eclipsed octahedral layers: it can be seen that the additional *c*-axis doubling is due to the slight staggering of the adjacent layers, in an antiferrodistortive style along the *b*-axis, presumably

caused by accommodation of the *inter*-layer species. Tremblay *et al.*[17] have discussed the nature and variable extent of staggering of octahedral layers (*i.e.* the transition from 'DJ-like' to 'RP-like'), which serves as a useful parameter for comparison of structures of this type. We can find no previous example of a similar $2a_p \times 2a_p \times 2c_p$ supercell for a LHP of $APbX_4$, A_2PbX_4 or $AA'PbX_4$ composition. The near-eclipsing of adjacent $[PbBr_4]_\infty$ layers leads to noticeably short *inter*-layer Br---Br non-bonded contacts of 4.096(1) Å. We can also find no previous examples of such a short *inter*-layer contacts in a single-layer LHP, although Ke *et al.*[18] suggest I---I distances of around 4.2 Å in some iodide members of this family.

The different distortion modes, *i.e.* the distinct octahedral tilting schemes and the presence or absence of staggering of adjacent layers, which occur in T_2PbBr_4 and related materials, are most easily identified using the on-line software ISODISTORT,[19] which uses a normal mode analysis: further details for T_2PbBr_4 are given in ESI. A similar analysis of all previously reported $APbX_4$ or A_2PbX_4 LHPs may be enlightening for the understanding of structure-directing effects of other amines, but this is beyond the scope of the present work.

Selected geometrical parameters and octahedral distortion parameters are given in Table 2. It can be seen that the two nitrogen atoms in the 1-position of the triazolium participate in two H-bonds each to Br; in contrast the two in the 4-position only donate a single H-bond to Br. There are no H-bonds between triazolium moieties (Table S2).

Table 2. Selected geometrical and octahedral distortion parameters at 298 K.

	T_2PbBr_4	**A_2PbBr_4**	**$ITPbBr_4$**	
	Pb1	Pb1	Pb1	Pb2
Pb-Br (Å)	2.9841(6)	2.8901(5)	3.0023(7)	2.9082(6)
	2.9924(3)	2.9141(5)	3.0024(7)	2.9082(6)
	3.0041(8)	2.9297(5)	3.0024(9)	3.0027(9)
	3.0055(7)	3.1395(5)	3.0130(9)	3.0127(9)
	3.0157(3)	3.2112(5)	3.0152(6)	3.1597(6)
	3.0282(7)	3.3221(5)	3.0152(6)	3.1598(6)
Pb-Br-Pb (°)	162.92(4)	162.35(2)	171.41(2)	
	165.82(3)	166.45(2)	179.53(4)	
	169.54(4)		180	
Br-Pb-Br range (°)	81.921(15)-97.984(15)	80.551(16)-99.560(16)	85.616(13)-94.384(13)	85.233(11)-94.767(11)

Δd (×10⁻⁴)	0.23	29.16	0.04	11.70
σ²	33.56	26.12	7.01	26.58

A_2PbBr_4

A_2PbBr_4 crystallises in a "corrugated 2 × 2 layer" (110)-oriented structure type (Figure 3). The unit cell and space group, $P2_1/c$, are consistent with a slight distortion of the framework (*i.e.* octahedral tilts and distortions) of the type seen in the first reported all-inorganic example of this structure type, $NdBaInO_4$.[20] The aristotype phase of the $AA'BX_4$ (110)-type (*i.e.* no octahedral tilting) has space group *Cmcm*, typified by $NdBaScO_4$.[6] This higher symmetry structure has not yet been seen amongst the known LHPs. The specific type of distortion (*i.e.* unit cell metrics and space group) seen here for A_2PbBr_4 has previously been observed in [(aminoethyl)isothiourea]$PbBr_4$[21] but this is the first example of a LHP with this structure type of the formula $AA'BX_4$.

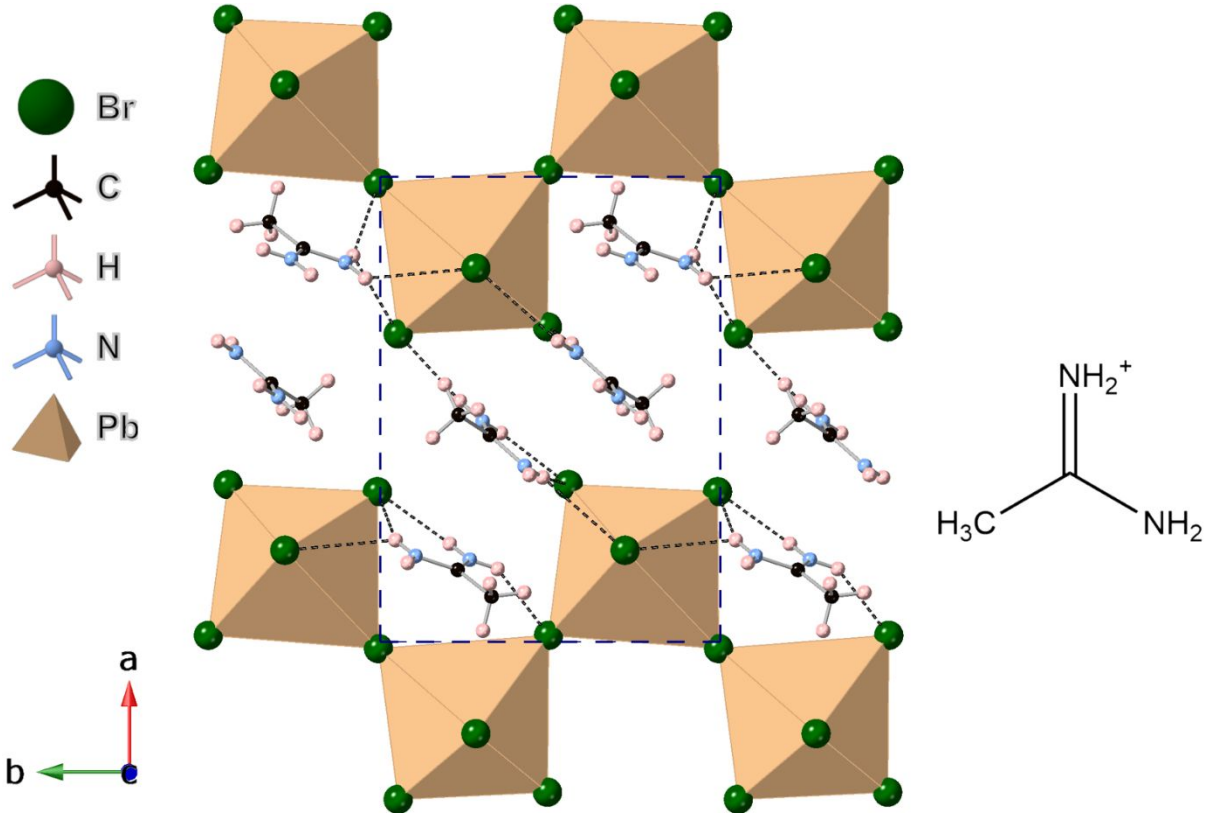

Figure 3. Crystal structure of A_2PbBr_4.

As is the case in T_2PbBr_4 there is only one crystallographically unique Pb site, but two distinct [AaH^+] sites. The *intra*-layer acetamidinium forms H-bonds only to the nearby $[PbBr_4]_\infty$ layer, whereas the *inter*-layer [AaH^+] forms H-bonds to adjacent inorganic layers *via* N1 and N2. Amongst the relatively small number of reported 2 × 2 (110)-oriented layered hybrid perovskites, we have found only six that have a stoichiometry AA′BX_4 rather than ABX_4.[7,8,22,23] Four of these contain guanidinium [GuH^+]: $[GuH]_2PbI_4$, $[GuH]_2SnI_4$, [ImH][GuH]$PbBr_4$ and [TzH][GuH]$PbBr_4$. The latter two examples are interesting as they show that [GuH^+] is capable of occupying either the *intra*-layer or *inter*-layer site, depending on competition between [GuH^+] and the second organic moiety. The occupation of both sites simultaneously by [GuH^+] has recently been reported in a related 3 × 1 (110)-oriented perovskite, $[GuH]_{1.5}$[4Me-ImH]$_{0.5}SnI_4$.[24] In [TzH][GuH]$PbBr_4$, it is perhaps surprising that [TzH^+] occupies the *intra*-layer site. This was discussed by Guo *et al.*[7]: the ionic sizes of [GuH^+] and [TzH^+] are approximately the same, and it was reasoned that *inter*-molecular[GuH^+]---[TzH^+] hydrogen bonds may play a significant role in stabilising the cation ordering in that case. Since [AaH^+] is anticipated to be approximately the same size as [GuH^+], it may be no surprise that A_2PbBr_4 adopts the (110)-oriented structure rather than any (001)-oriented option. The H-bonding options are, of course, more restricted for [AaH^+] versus [GuH^+], nevertheless Figure 3 and Table S4 show that there is *inter*-layer H-bonding present here *via* the *inter*-layer [AaH^+].

Selected geometrical parameters for A_2PbBr_4 are given in Table 2. Although there are currently only a small number of (110)-oriented LHPs, these display quite a diversity of specific structural distortions (*i.e.* unit cell metrics and space groups derived from the aristotype phase). We therefore offer no universal trends regarding the nature of these distortions versus compositional features, in terms of *inter*-layer interactions and other longer-range structural features. Moreover, there appears little systematic behaviour regarding the local structural features within this family, such as the level of individual PbX_6 octahedral distortions and *inter*-octahedral angles. Amongst the known (110)-oriented structure layered hybrid perovskites of AA'BX_4 stoichiometry, A_2PbBr_4 is seen to exhibit the largest octahedral distortions and amongst the largest *inter*-octahedral distortions (*i.e.* B-X-B bond angles, Table 3). This is seen, for example, in comparing to the two previous A_2BX_4 compositions, $[GuH]_2PbI_4$ and $[GuH]_2SnI_4$, in their monoclinic polymorphs, which exist close to room temperature: these compounds show the largest *inter*-octahedral distortions of this family. Surprisingly, and for reasons we cannot explain, perhaps the closest compositional analogue to A_2PbBr_4, $[GuH]_2PbBr_4$ does not adopt a (110)-oriented structure, instead preferring an unusual chain-

like structure.[25] The series of [3APr]PbX_4 structures,[26] for X = Cl, Br, I, are also compared in Table 3. This also suggests little direct correlation of distortion parameters versus the nature of X, based on the existing small dataset.

Table 3. Octahedral and *inter*-octahedral distortions of known (110)-oriented layered hybrid perovskites.

	Δd ($\times 10^{-4}$)	σ^2	B-X-B (°)
A_2PbBr_4	29.16	26.12	162.35(2)
			166.45(2)
[ImH][GuH]$PbBr_4$[7]	8.91	7.71	178.10(7)
			180
[TzH][GuH]$PbBr_4$[7]	7.59	22.06	171.51(3)
			180
[FA][HEA]$PbBr_4$[8]	5.70	11.59	173.13(6)
	13.66	14.46	177.96(4)
$[GuH]_2PbI_4$[22]	7.78	12.65	154.27(2)
			157.35(2)
	11.16	8.41	158.42(2)
			176.06(2)
$[GuH]_2SnI_4$[22]	20.06	6.78	157.08(2)
			159.63(2)
	23.47	6.14	161.48(2)
			177.10(2)
[IFA][MA]SnI_4[23]	2.02	7.77	173.30(10)
			180
[3APr]$PbCl_4$[26]	12.32	34.50	169.70
			170.50
[3APr]$PbBr_4$[26]	9.81	21.07	171.31
			173.24
[3APr]PbI_4[26]	11.92	22.04	169.58
			178.18

$ITPbBr_4$

$ITPbBr_4$ adopts an unusual variant of the (110)-oriented structure, which has also been described as a "corrugated 3 × 3 layer" structure. This structure type contains rows of alternating *cis*- and *trans*-shared octahedra linked into (110) sheets (Figure 4). There are only four previously reported examples of this structure type: [α-DMEN]$PbBr_4$ ($[DMEN]^{2+}$ = 2-(dimethylamino)ethylammonium),[3] [ImEA]PbI_4 ($[ImEA]^{2+}$ = imidazoliumethylammonium)[27] and [4NPEA]PbX_4 (X = Br or I; 4NPEA = 4-nitrophenylethylammonium).[28] $ITPbBr_4$ is

therefore the first example of a bromide of this structure type incorporating two distinct molecular species. The two distinct types of PbX_6 octahedra (*i.e. cis*- and t*rans*- ligands being terminal, respectively) in each case show very different degrees of distortion, with the *trans* site being much more regular (Table 2).

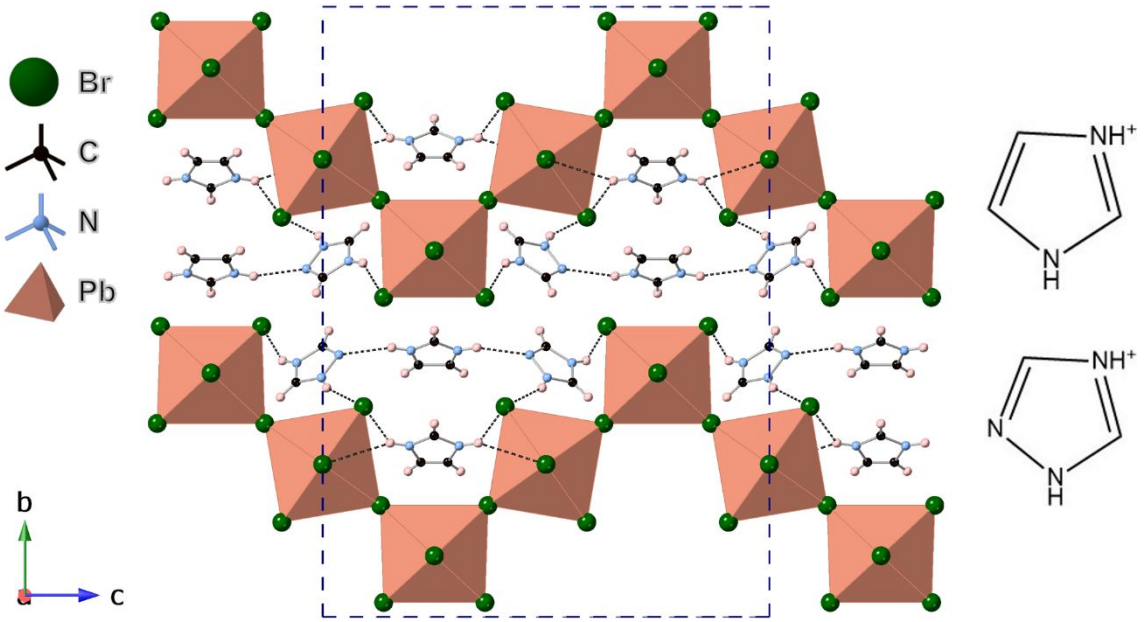

Figure 4. Crystal structure of $ITPbBr_4$.

The unit cell metrics of this type of structure, in its simplest form, are characterised by two axial lengths determined by the geometry of the linked PbX_6 octahedra and one dictated by the packing of the adjacent layers, and the nature of the *inter*-layer moieties. Thus, an axial length of around 19 Å along the corrugation direction of the $[PbX_4]_\infty$ sheet (*c*-axis in $ITPbBr_4$, Fig 4) arises from the lateral edge-to-edge width of four linked octahedra. A length of about 6 Å derives from the Pb-Br-Pb distance between two vertex-linked octahedra perpendicular to this (*a*-axis in $ITPbBr_4$), and a variable *inter*-layer distance is dictated by the nature and packing of the organic moieties ($b \sim 26$ Å in $ITPbBr_4$). By comparing the metrics of the known examples of this structure type (Table S9), it can be seen that $ITPbBr_4$ has one the 'simplest' variants of this basic unit cell, exhibiting the simple 6 Å metric perpendicular to the corrugation direction, whereas each of the other examples has a doubled axis, due to octahedral tilting. Interestingly, only one example ($[ImEA]PbI_4$) has a structure where the *inter*-layer unit cell axis represents the distance between adjacent $[PbX_4]_\infty$ sheets: each of the others has a doubled axis here, apparently due to alternating orientations of the *inter*-layer moieties.

There are no direct *inter*-layer links *via* H-bonding in $ITPbBr_4$, although there are $[ImH^+]$---$[TzH^+]$ H-bonds between the moieties that are both interacting with the same $[PbBr_4]_\infty$ sheet. Since our previous study[7] suggested that $[ImH^+]$ and $[TzH^+]$ are approximately the same size, it seems that these H-bonding preferences may play a subtle role in dictating the observed cation ordering (*i.e.* ordering of $[ImH^+]$ into the *intra*-layer sites in this structure) although this suggestion can only be speculative. Indeed, the features that favour the adoption of the 3 × 3 layer structure itself, rather than some of the possible competing polymorphs, are not clear from the limited amount of data available at this stage. It is likely that the energy landscapes discriminating different polymorphs in some of these systems are rather 'flat', for example $[DMEN]PbBr_4$ crystallises in two distinct polymorphs, the thermodynamically stable α-phase, having the 3 × 3 layer structure and the β-phase, the kinetic product, having a (001) layer structure.[3]

Photophysical Properties

UV-Vis

All three absorption spectra (Figure 5) revealed features similar to previously reported 2D layered LHPs, *viz.*, two separated absorption peaks.[7,29–31] That is, T_2PbBr_4 has two absorption peaks at 3.05 eV (407 nm) and 2.85 eV (435 nm), $ITPbBr_4$ has peaks at 3.27 eV (379 nm) and 3.02 eV (411 nm) and A_2PbBr_4 has peaks at 3.56 eV (348 nm) and 3.29 eV (377 nm).

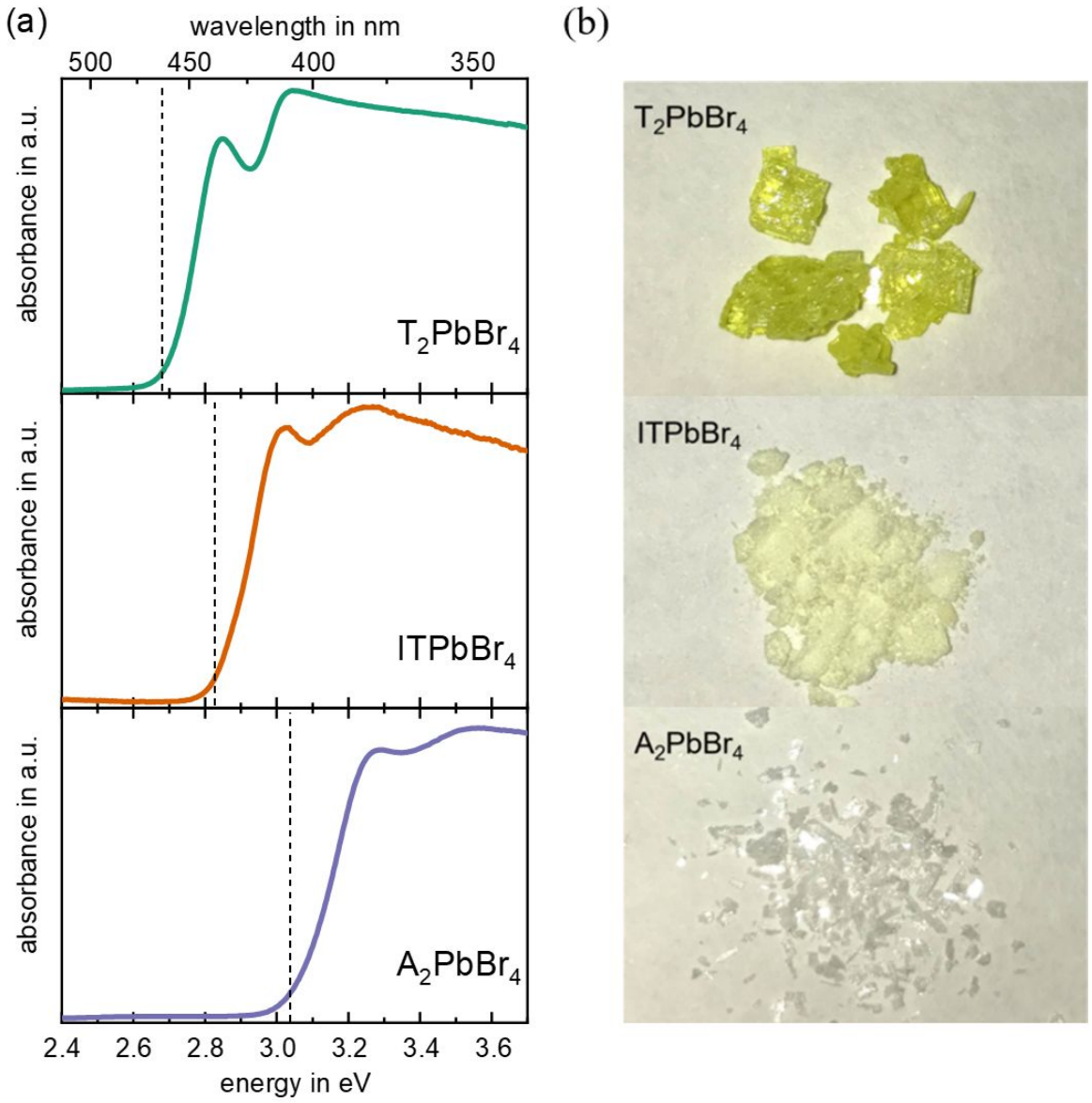

Figure 5. (a) UV-Vis absorption spectra of T_2PbBr_4, $ITPbBr_4$ and A_2PbBr_4 and at room temperature; the dashed lines indicate the energy of the absorption onset and (b) crystals of T_2PbBr_4, $ITPbBr_4$ and A_2PbBr_4.

From these spectra, it also becomes clear that the energetic spacing between the two peaks increases from 0.20 eV and 0.25 eV to 0.27 eV for T_2PbBr_4 and $ITPbBr_4$ to A_2PbBr_4 respectively. The peaks at lower energies can be attributed to exciton absorption in each system,[32,33] which precludes extracting the fundamental band gap with the help of a Tauc plot.[34] We thus estimate the optical gap from the absorption onset (dashed lines in Figure 5a), which increases from 2.68 eV (463 nm) and 2.82 eV (440 nm), to 3.03 eV (409 nm) when going from T_2PbBr_4 and $ITPbBr_4$ to A_2PbBr_4, respectively. Both the increasing optical gap together with

the increasing energetic spacing between the two absorption peaks are in agreement with the idea of a greater electronic confinement,[35,36] with the spread of the electron wavefunction being inhibited where the connectivity between neighboring octahedra change between *cis*- and *trans*- conformation ($ITPbBr_4 < A_2PbBr_4$).[37] While the increase in optical gap essentially stems from the "particle in a box" solution to the Schrödinger equation,[38] the increased spacing between the absorption peaks reflects an increased exciton binding energy with greater confinement. Correspondingly, the colors of the three materials change from bright yellow (T_2PbBr_4) to pale yellow ($ITPbBr_4$) and then to white (A_2PbBr_4) (Figure 5b).

PL spectra

Figure 6 shows the normalized PL spectra of all three compounds when they are excited at 3.67 eV (337 nm). The emission spectrum of T_2PbBr_4 shows two distinct sharp peaks at 2.68 eV (463 nm) and 2.85 eV (435 nm). The emission spectrum of A_2PbBr_4 shows a different behavior with a broad peak at ~ 1.97 eV (628 nm), corresponding to a large energetic spacing between the PL peak and the absorption peak at 3.29 eV (377 nm). Furthermore, the full width at half-maximum (FWHM) of the broad PL peak is ~ 0.72 eV (240 nm). In contrast, two PL peaks are observed in the case of $ITPbBr_4$. The dominating broad signal at 1.92 eV (647 nm) has essentially the same shape as the PL of A_2PbBr_4, and the PL peak at 2.75 eV (451 nm) is in the energetic range similar to the emission of T_2PbBr_4. We measured the photoluminescence quantum efficiency PLQY at room temperature and found it to be below 1% for all three samples. While these values are low compared to the highest reported PLQYs of low dimensional lead bromide perovskites,[29,39] several works also report comparably low PLQYs.[40,41]

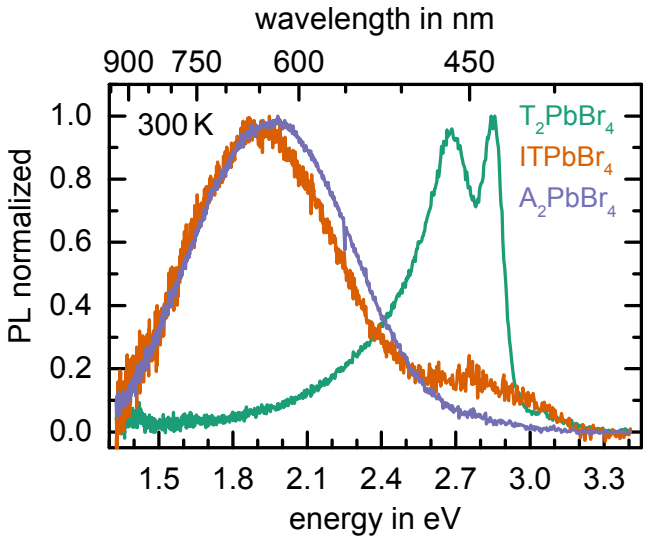

Figure 6. Normalized PL spectra (excited at 337 nm) for T_2PbBr_4, $ITPbBr_4$and A_2PbBr_4 at room temperature.

To better understand the origin of the different emitting states, temperature-dependent steady-state PL measurements were performed from 300 K to 120 K (20 K intervals) for all three compounds.

Figure 7 shows the temperature-dependent PL spectra for each perovskite system. For all materials, the overall PL intensity increases upon cooling to 120 K. For T_2PbBr_4, the peak at 2.68 eV (463 nm) at 300 K gradually shifts to higher energies upon cooling to 200 K (Figure 7a). From 200 K onwards, it retains its position and raises in intensity, becoming the dominant PL feature at 120 K. Further, an additional low energy emission band (~1.87 eV, 663 nm) appears at temperatures below 160 K.

As mentioned above, $ITPbBr_4$ shows two emissive features, where the peak at higher energies (2.80 eV, 443 nm) exhibits a low relative intensity compared to the PL feature at lower energies at room temperature (Figure 7b). Upon cooling, the ratio between the PL peaks at high and low energy decreases. The emission band at lower energy (1.89 eV, 656 nm) remains the dominant PL feature in the entire investigated temperature range, where its FWHM narrows from 0.72 eV (258 nm) at 300 K to 0.46 eV (173 nm) at 120 K. Additionally, we observe that the high energy band becomes more structured at low temperatures, exhibiting several distinct PL features at similar peak positions compared to the high energy PL features of T_2PbBr_4. PL of A_2PbBr_4 predominantly exhibits the low energy emission at ~ 1.97 eV in the investigated temperature range between 300 K and 120 K (Figure 7c). Upon cooling, the FWHM of the PL

peak continuously reduces from 0.72 eV (240 nm) at RT to 0.48 eV (154 nm) at 120 K, while its energetic position remains constant. Below 200 K, a weak PL at energies > 2.8 eV (443 nm) appears. Compared to the PL band at ~ 1.97 eV, its intensity is lower by more than three orders of magnitude.

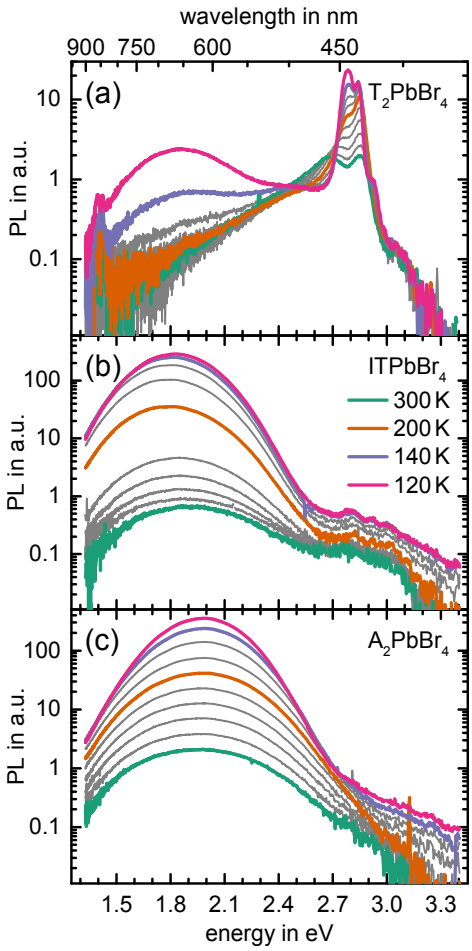

Figure 7. Temperature-dependent (300-120 K) steady-state PL spectra of (a) T_2PbBr_4, (b) $ITPbBr_4$ and (c) A_2PbBr_4.

The results of the PL measurements suggest two different emitting species since the high energy signal in T_2PbBr_4 is rather narrow and structured, whereas the emission at lower energies is broad and significantly separated in energy from corresponding absorption onsets. The PL peak at 2.85 eV (435 nm) is nearly resonant with the exciton absorption shown in Figure 5, so that we associate this high energy PL band with exciton recombination.[42,43] Broad emission features at low photon energies are often observed in 2D-perovskite systems,[44–47] and it was suggested that they stem from recombination via intrinsic (electron-phonon

coupling) or extrinsic (electron-lattice defect) self-trapped excitons (STE).[40,48] This may also be a possible interpretation for the observed emission at lower energies of the materials investigated in our case. In contrast, we deem the occurrence of the low energy features due to a possible structural phase transition at low temperatures to be rather unlikely. In such a case, we would expect a decrease of the PL signals associated to the high temperature phase, the abrupt appearance of low temperature phase PL features, also with a similar spectral width compared to the high temperature phase PL features.[49] Typically this all would happen within a relatively small temperature range.[50]

The ratio between the high and low energy bands is temperature dependent, *i.e.* reflecting some thermally activated detrapping process.[40,51] Nevertheless, overall, we observe a stronger dominance of the low energy band along the series from T_2PbBr_4 over $ITPbBr_4$ to A_2PbBr_4. This is in line with reports from literature showing that broad PL at low energies can be facilitated by an increase of distortions and corrugation.[44,45] Considering that the energy differences between high and low energy bands are fairly similar for all three systems, the lower intensity of the broad peak is likely to reflect a lower density of STE states in T_2PbBr_4 than in $ITPbBr_4$ and A_2PbBr_4. In the literature, a change in the PL intensity between high and low energy PL bands was associated with a change in the energy difference between the absorption onset and the energy of the STE emission.[26,52] It was suggested that a smaller energy difference is favourable for STE detrapping leading to an increased PL intensity of the high energy band. This at first sight is in line with our results, however such a thermal detrapping process appears questionable to us, as the observed energy difference between low and high energy PL bands is large (~0.7 eV) compared to thermal energy. Furthermore a recent study shows that the low energy PL band originates from in-gap states, rather than being due to STEs,[53] which emphasizes the general need for more detailed future studies.

Conclusions

We have prepared three new examples of hybrid lead bromide layered perovskites of different structural variations templated using small disc-shaped amines. The cationic ordering behaviour of each composition have been discussed in terms of ionic size effects and hydrogen-bonding environments. In T_2PbBr_4 we introduce a previously unreported 'DJ-like' (001)-oriented structure type with a $2a_p \times 2a_p \times 2c_p$ supercell arising from octahedral tilting and the arrangement of the $[TzH^+]$ moieties. The two (110)-oriented perovskites reported, A_2PbBr_4 and

$ITPbBr_4$, represent two new examples of this rare structure-type featuring corrugation patterns of 2 × 2 and 3 × 3, respectively. The octahedral distortions present in A_2PbBr_4 are the largest reported for any material of the 2 × 2 type, however we are unable to identify any systematic behaviour amongst known (110)-oriented structures to explain this. $ITPbBr_4$ is the first example of a bromide 3 × 3 type structure incorporating two distinct molecular species and represents the 'simplest' variant of the basic unit cell among known materials of this structure type. All three materials exhibit peaks consistent with exciton absorption in UV-vis spectroscopy. Photoluminescence data indicate a distinct change in behaviour with increasing structural corrugation. In T_2PbBr_4, there is a narrow and structured emission observed at higher energies attributed to exciton recombination, as well as a broad emission at lower energies corresponding to recombination *via* extrinsic or intrinsic STE. With the increasing structural distortions and corrugation in $ITPbBr_4$ and A_2PbBr_4, the broad emission feature dominates. The diverse structures and photoluminescent behaviour exhibited in these materials obtained from similar disc-shaped amines highlights the need for greater exploration and study of hybrid layered perovskites towards potential functionalities.

Supporting Information

Crystallographic data at 173 K, hydrogen bonding details, octahedral distortion parameters, brief review of (110)-oriented layered perovskite unit cell details, ISODISTORT mode amplitudes for T_2PbBr_4.

The research data pertaining to this paper are available at https://doi.org/10.17630/54781f80-3c71-48a2-aed7-45381cab7683

Acknowledgments

We thank Prof. E. Zysman-Colman and Prof. Anna Köhler for helpful suggestions throughout. Y.-Y.G. and T.L. acknowledge the University of St Andrews and China Scholarship Council for funding of studentships (201603780005) and (201606280032), respectively. J.A.M. and P.L. acknowledge financial support from the Leverhulme trust (RPG-2018-065). S.B., K.S. and F.P. acknowledge financial support from the German National Science Foundation via the Projects 423895689, KO 3973/2-1 and PA 3373/3-1 and further acknowledge support by the Bavarian State Ministry of Science, Research, and the Arts for the Collaborative Research Network ''Solar Technologies go Hybrid''.

REFERENCES

(1) Saparov, B.; Mitzi, D. B. Organic-Inorganic Perovskites: Structural Versatility for Functional Materials Design. *Chem. Rev.* **2016**, *116* (7), 4558–4596.

(2) Smith, M. D.; Crace, E. J.; Jaffe, A.; Karunadasa, H. I. The Diversity of Layered Halide Perovskites. *Annu. Rev. Mater. Res.* **2018**, *48* (1), 111–136.

(3) Mao, L.; Wu, Y.; Stoumpos, C. C.; Wasielewski, M. R.; Kanatzidis, M. G. White-Light Emission and Structural Distortion in New Corrugated Two-Dimensional Lead Bromide Perovskites. *J. Am. Chem. Soc.* **2017**, *139* (14), 5210–5215.

(4) Benedek, N. A.; Rondinelli, J. M.; Djani, H.; Ghosez, P.; Lightfoot, P. Understanding Ferroelectricity in Layered Perovskites: New Ideas and Insights from Theory and Experiments. *Dalton Trans.* **2015**, *44* (23), 10543–10558.

(5) Balachandran, P. V; Young, J.; Lookman, T.; Rondinelli, J. M. Learning from Data to Design Functional Materials without Inversion Symmetry. *Nat. Commun.* **2017**, *8*, 1–13.

(6) Cochrane, A. K.; Telfer, M.; Dixon, C. A. L.; Zhang, W.; Halasyamani, P. S.; Bousquet, E.; Lightfoot, P. $NdBaScO_4$: Aristotype of a New Family of Geometric Ferroelectrics? *Chem. Commun.* **2016**, *52* (73), 10980–10983.

(7) Guo, Y. Y.; McNulty, J. A.; Mica, N. A.; Samuel, I. D. W.; Slawin, A. M. Z.; Bühl, M.; Lightfoot, P. Structure-Directing Effects in (110)-Layered Hybrid Perovskites Containing Two Distinct Organic Moieties. *Chem. Commun.* **2019**, *55* (67), 9935–9938.

(8) Salah, M. B. H.; Mercier, N.; Allain, M.; Zouari, N.; Giovanella, U.; Botta, C. Mechanochromic and Electroluminescence Properties of a Layered Hybrid Perovskite Belonging to the <110> Series. *Eur. J. Inorg. Chem.* **2019**, *2019* (42), 4527–4531.

(9) Febriansyah, B.; Giovanni, D.; Ramesh, S.; Koh, T. M.; Li, Y.; Sum, T. C.; Mathews, N.; England, J. Inducing Formation of a Corrugated, White-Light Emitting 2D Lead-Bromide Perovskite via Subtle Changes in Templating Cation . *J. Mater. Chem. C* **2020**, *8* (110), 889–893.

(10) Rigaku. Rigaku Corporation, Tokyo, Japan. *CrystalClear*. 2014.

(11) Sheldrick, G. M. Crystal Structure Refinement with SHELXL. *Acta Cryst. C* **2015**, *71*, 3–8.

(12) Farrugia, L. J. WinGX and ORTEP for Windows: An Update. *J. Appl. Crystallogr.* **2012**, *45* (4), 849–854.

(13) Schötz, K.; Askar, A. M.; Peng, W.; Seeberger, D.; Gujar, T. P.; Thelakkat, M.; Köhler, A.; Huettner, S.; Bakr, O. M.; Shankar, K.; et al. Double Peak Emission in Lead Halide Perovskites by Self-Absorption. *J. Mater. Chem. C* **2020**, *8* (7), 2289–2300.

(14) de Mello, J. C.; Wittmann, H. F.; Friend, R. H. An Improved Experimental Determination of External Photoluminescence Quantum Efficiency. *Adv. Mater.* **1997**, *9* (3), 230–232.

(15) Mercier, N. Hybrid Halide Perovskites: Discussions on Terminology and Materials. *Angew. Chemie - Int. Ed.* **2019**, *58* (50), 17912–17917.

(16) Li, T.; Clulow, R.; Bradford, A. J.; Lee, S. L.; Slawin, A. M. Z.; Lightfoot, P. A Hybrid Fluoride Layered Perovskite, $(enH_2)MnF_4$. *Dalton Trans.* **2019**, *48* (15), 4784–4787.

(17) Tremblay, M.-H.; Bacsa, J.; Zhao, B.; Pulvirenti, F.; Barlow, S.; Marder, S. R. Structures of $(4\text{-}Y\text{-}C_6H_4CH_2NH_3)_2PbI_4$ {Y = H, F, Cl, Br, I}: Tuning of Hybrid Organic Inorganic Perovskite Structures from Ruddlesden–Popper to Dion–Jacobson Limits. *Chem. Mater.* **2019**, *31* (16), 6145–6153.

(18) Ke, W.; Mao, L.; Stoumpos, C. C.; Hoffman, J.; Spanopoulos, I.; Mohite, A. D.; Kanatzidis, M. G. Compositional and Solvent Engineering in Dion-Jacobson 2D Perovskites Boosts Solar Cell Efficiency and Stability. *Adv. Energy Mater.* **2019**, *9* (10), 1803384.

(19) Campbell, B. J.; Stokes, H. T.; Tanner, D. E.; Hatch, D. M. ISODISPLACE: A Web-Based Tool for Exploring Structural Distortions. *J. Appl. Crystallogr.* **2006**, *39* (4), 607–614.

(20) Fujii, K.; Esaki, Y.; Omoto, K.; Yashima, M.; Hoshikawa, A.; Ishigaki, T.; Hester, J. R. New Perovskite-Related Structure Family of Oxide-Ion Conducting Materials $NdBaInO_4$. *Chem. Mater.* **2014**, *26* (8), 2488–2491.

(21) Li, Y.; Zheng, G.; Lin, J. Synthesis, Structure, and Optical Properties of a Contorted 〈110〉-Oriented Layered Hybrid Perovskite: $C_3H_{11}SN_3PbBr_4$. *Eur. J. Inorg. Chem.* **2008**, *4* (10), 1689–1692.

(22) Daub, M.; Haber, C.; Hillebrecht, H. Synthesis, Crystal Structures, Optical Properties, and Phase Transitions of the Layered Guanidinium-Based Hybrid Perovskites $[C(NH_2)_3]_2MI_4$; M = Sn, Pb. *Eur. J. Inorg. Chem.* **2017**, *2017* (7), 1120–1126.

(23) Mitzi, D. B.; Wang, S.; Feild, C. A.; Chess, C. A.; Guloy, A. M. Conducting Layered Organic-Inorganic Halides Containing 〈110〉-Oriented Perovskite Sheets. *Science* **1995**, *267* (5203), 1473–1476.

(24) McNulty, J. A.; Lightfoot, P. Unprecedented Tin Iodide Perovskite-like Structures Featuring Ordering of Organic Moieties. *Chem. Commun.* **2020**, *56*, 4543–4546.

(25) Nazarenko, O.; Kotyrba, M. R.; Wörle, M.; Cuervo-Reyes, E.; Yakunin, S.; Kovalenko, M. V. Luminescent and Photoconductive Layered Lead Halide Perovskite Compounds Comprising Mixtures of Cesium and Guanidinium Cations. *Inorg. Chem.* **2017**, *56* (19), 11552–11564.

(26) Li, X.; Guo, P.; Kepenekian, M.; Hadar, I.; Katan, C.; Even, J.; Stoumpos, C. C.; Schaller, R. D.; Kanatzidis, M. G. Small Cyclic Diammonium Cation Templated (110)-Oriented 2D Halide (X = I, Br, Cl) Perovskites with White-Light Emission. *Chem. Mater.* **2019**, *31* (9), 3582–3590.

(27) Febriansyah, B.; Koh, T. M.; Lekina, Y.; Jamaludin, N. F.; Bruno, A.; Ganguly, R.; Shen, Z. X.; Mhaisalkar, S. G.; England, J. Improved Photovoltaic Efficiency and Amplified Photocurrent Generation in Mesoporous n = 1 Two-Dimensional Lead-Iodide Perovskite Solar Cells. *Chem. Mater.* **2019**, *31* (3), 890–898.

(28) Tremblay, M. H.; Thouin, F.; Leisen, J.; Bacsa, J.; Srimath Kandada, A. R.; Hoffman, J. M.; Kanatzidis, M. G.; Mohite, A. D.; Silva, C.; Barlow, S.; et al. $(4NPEA)_2PbI_4$ (4NPEA = 4-Nitrophenylethylammonium): Structural, NMR, and Optical Properties of a 3 × 3 Corrugated 2D Hybrid Perovskite. *J. Am. Chem. Soc.* **2019**, *141* (11), 4521–4525.

(29) Dohner, E. R.; Jaffe, A.; Bradshaw, L. R.; Karunadasa, H. I. Intrinsic White-Light Emission from Layered Hybrid Perovskites. *J. Am. Chem. Soc.* **2014**, *136* (38), 13154–13157.

(30) Gautier, R.; Massuyeau, F.; Galnon, G.; Paris, M. Lead Halide Post-Perovskite-Type Chains for High-Efficiency White-Light Emission. *Adv. Mater.* **2019**, *31* (14), 6–11.

(31) Nazarenko, O.; Kotyrba, M. R.; Yakunin, S.; Aebli, M.; Rainò, G.; Benin, B. M.; Wörle, M.; Kovalenko, M. V. Guanidinium-Formamidinium Lead Iodide: A Layered Perovskite-Related Compound with Red Luminescence at Room Temperature. *J. Am. Chem. Soc.* **2018**, *140* (11), 3850–3853.

(32) Stoumpos, C. C.; Soe, C. M. M.; Tsai, H.; Nie, W.; Blancon, J. C.; Cao, D. H.; Liu, F.; Traoré, B.; Katan, C.; Even, J.; et al. High Members of the 2D Ruddlesden-Popper Halide Perovskites: Synthesis, Optical Properties, and Solar Cells of $(CH_3(CH_2)_3NH_3)_2(CH_3NH_3)_4Pb_5I_{16}$. *Chem* **2017**, *2* (3), 427–440.

(33) Cao, D. H.; Stoumpos, C. C.; Farha, O. K.; Hupp, J. T.; Kanatzidis, M. G. 2D Homologous Perovskites as Light-Absorbing Materials for Solar Cell Applications. *J. Am. Chem. Soc.* **2015**, *137* (24), 7843–7850.

(34) Green, M. A.; Jiang, Y.; Soufiani, A. M.; Ho-Baillie, A. Optical Properties of Photovoltaic Organic-Inorganic Lead Halide Perovskites. *J. Phys. Chem. Lett.* **2015**, *6* (23), 4774–4785.

(35) Dohner, E. R.; Hoke, E. T.; Karunadasa, H. I. Self-Assembly of Broadband White-Light Emitters. *J. Am. Chem. Soc.* **2014**, *136* (5), 1718–1721.

(36) Lermer, C.; Harm, S. P.; Birkhold, S. T.; Jaser, J. A.; Kutz, C. M.; Mayer, P.; Schmidt-Mende, L.; Lotsch, B. V. Benzimidazolium Lead Halide Perovskites: Effects of Anion Substitution and Dimensionality on the Bandgap. *Zeitschrift fur Anorg. und Allg. Chemie* **2016**, *642* (23), 1369–1376.

(37) Tong, Y.; Bladt, E.; Aygüler, M. F.; Manzi, A.; Milowska, K. Z.; Hintermayr, V. A.; Docampo, P.; Bals, S.; Urban, A. S.; Polavarapu, L.; et al. Highly Luminescent Cesium Lead Halide Perovskite Nanocrystals with Tunable Composition and Thickness by Ultrasonication. *Angew. Chemie - Int. Ed.* **2016**, *55* (44), 13887–13892.

(38) Parrott, E. S.; Patel, J. B.; Haghighirad, A. A.; Snaith, H. J.; Johnston, M. B.; Herz, L. M. Growth Modes and Quantum Confinement in Ultrathin Vapour-Deposited $MAPbI_3$ Films. *Nanoscale* **2019**, *11* (30), 14276–14284.

(39) Gong, X.; Voznyy, O.; Jain, A.; Liu, W.; Sabatini, R.; Piontkowski, Z.; Walters, G.; Bappi, G.; Nokhrin, S.; Bushuyev, O.; et al. Electron-Phonon Interaction in Efficient Perovskite Blue Emitters. *Nat. Mater.* **2018**, *17* (6), 550–556.

(40) Smith, M. D.; Karunadasa, H. I. White-Light Emission from Layered Halide Perovskites. *Acc. Chem. Res.* **2018**, *51* (3), 619–627.

(41) Shin, D. H.; Ko, J. S.; Kang, S. K.; Choi, S. H. Enhanced Flexibility and Stability in Perovskite Photodiode-Solar Cell Nanosystem Using MoS_2 Electron-Transport Layer. *ACS Appl. Mater. Interfaces* **2020**, *12* (4), 4586–4593.

(42) Kitazawa, N.; Aono, M.; Watanabe, Y. Temperature-Dependent Time-Resolved Photoluminescence of $(C_6H_5C_2H_4NH_3)_2PbX_4$ (X = Br and I). *Mater. Chem. Phys.* **2012**, *134* (2–3), 875–880.

(43) Kitazawa, N.; Ito, T.; Sakasegawa, D.; Watanabe, Y. Excitons in Self-Organized Layered Perovskite Films Prepared by the Two-Step Growth Process. *Thin Solid Films* **2006**, *500* (1–2), 133–137.

(44) Lin, H.; Zhou, C.; Tian, Y.; Siegrist, T.; Ma, B. Low-Dimensional Organometal Halide Perovskites. *ACS Energy Lett.* **2018**, *3* (1), 54–62.

(45) Cortecchia, D.; Yin, J.; Petrozza, A.; Soci, C. White Light Emission in Low-Dimensional Perovskites. *J. Mater. Chem. C* **2019**, *7* (17), 4956–4969.

(46) Mott, N. F.; Stoneham, A. M. The Lifetime of Electrons, Holes and Excitons before Self-

Trapping. *J. Phys. C Solid State Phys.* **1977**, *10* (17), 3391–3398.

(47) Yin, J.; Li, H.; Cortecchia, D.; Soci, C.; Brédas, J. L. Excitonic and Polaronic Properties of 2D Hybrid Organic-Inorganic Perovskites. *ACS Energy Lett.* **2017**, *2* (2), 417–423.

(48) Nagami, A.; Okamura, K.; Ishihara, T. Optical Properties of a Quantum Wire Crystal, C5H10NH2PbI3. *Phys. B Condens. Matter* **1996**, *227* (1–4), 346–348.

(49) Schötz, K.; Askar, A. M.; Köhler, A.; Shankar, K.; Panzer, F. Investigating the Tetragonal-to-Orthorhombic Phase Transition of Methylammonium Lead Iodide Single Crystals by Detailed Photoluminescence Analysis. *Adv. Opt. Mater.* **2020**, *2000455*, 1–9.

(50) Panzer, F.; Li, C.; Meier, T.; Köhler, A.; Huettner, S. Impact of Structural Dynamics on the Optical Properties of Methylammonium Lead Iodide Perovskites. *Adv. Energy Mater.* **2017**, *7* (16), 1–11.

(51) Smith, M. D.; Jaffe, A.; Dohner, E. R.; Lindenberg, A. M.; Karunadasa, H. I. Structural Origins of Broadband Emission from Layered Pb-Br Hybrid Perovskites. *Chem. Sci.* **2017**, *8* (6), 4497–4504.

(52) Gautier, R.; Paris, M.; Massuyeau, F. Exciton Self-Trapping in Hybrid Lead Halides: Role of Halogen. *J. Am. Chem. Soc.* **2019**, *141* (32), 12619–12623.

(53) Kahmann, S.; Tekelenburg, E. K.; Duim, H.; Kamminga, M. E.; Loi, M. A. Extrinsic Nature of the Broad Photoluminescence in Lead Iodide-Based Ruddlesden–Popper Perovskites. *Nat. Commun.* **2020**, *11* (1), 1–8.

For Table of Contents Only

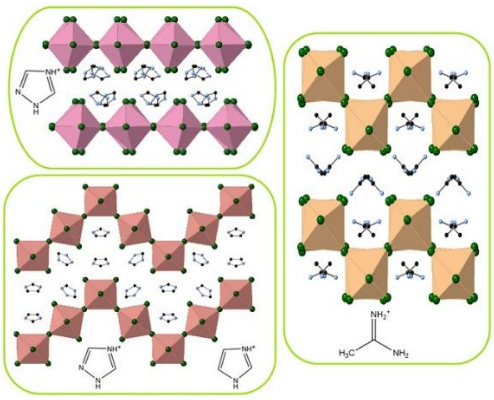

Combinations of two disc-shaped small amines template a diversity of layered lead halide perovskites